ChemComm

High gain, low loss, and low-threshold spherical organic laser based on highly miscible excited-state intramolecular proton transfer dyes

Journal:	*ChemComm*
Manuscript ID	CC-COM-12-2024-006784.R1
Article Type:	Communication

ChemComm

COMMUNICATION

High gain, low loss, and low-threshold spherical organic laser based on highly miscible excited-state intramolecular proton transfer dyes

Received 00th January 20xx,
Accepted 00th January 20xx

DOI: 10.1039/x0xx00000x

Shunya Aoyagi,[a] Yoshiya Omori,[b] Tsukasa Kawamura,[b] Tsuneaki Sakurai,*[b] Masaki Shimizu,[b] Kenichi Yamashita,[c] Yuki Nagai,[d] Yoichi Kobayashi,[d] Yohei Yamamoto*[,a] and Hiroshi Yamagishi*[a]

Here we report two types of excited-state intramolecular proton transfer dyes featuring exceptionally high misciblity with a polymer matrix (> 50 wt%). Using these dyes, we assemble spherical laser oscillators and observe a significant reduction in the laser emission threshold at higher dye concentrations due to the enhanced optical gain as well as supressed self-absorption and light scattering.

Organic whispering gallery mode (WGM) resonators have garnered increasing attention in recent years as a novel class of laser oscillators.[1] Typically, these lasers are minute spherical particles of an organic polymer doped with an emissive dye assembled together through emulsion polymerization or self-assembly in the solution phase. These lasers are characterized by their conciseness, wireless operation, and additional unique functionalities, such as biocompatibility and processability, derived from the constituent organic materials.[2,3]

Through the improvements of the dyes and polymers, the performances of the organic WGM lasers have been advanced a lot in the last decade particularly in lowering the lasing threshold.[4,5] To further reduce the threshold, recent studies have concentrated on the molecular design of the dyes for achieving a higher photoluminescent quantum yield (PLQY) and enhanced optical robustness, which are well-summarized in previous reports and reviews.[6,7]

In this study, we tackle this topic using a distinct molecular strategy, namely, enrichment of the emissive dye. A traditional laser theory predicts that the efficiency of laser emission can be improved simply by enriching the concentration of the gain molecules in a unit volume.[8,9] Despite its simplicity, this approach has been inapplicable to the organic WGM resonators due to the self-absorption and the immiscibility of the dye to the polymer matrix.

It is well-known that the emission band of an organic dye partially overlaps with its absorption band, causing self-absorption.[10] While this effect is usually negligible, it is critical in laser oscillators, where light travels along the circumference of the resonator iteratively, amplifying the effects of self-absorption.[11] Furthermore, excessive doping beyond the miscibility limit induces the aggregation of the dye within the polymer matrix, forming microcrystals or dye-rich domains. These aggregates scatter light inside the resonator and compromise the smoothness of the resonator surface, thereby inhibiting the efficient laser oscillation.[12]

Excited-state intramolecular proton transfer (ESIPT) dyes can be a candidate to overcome the first concern. ESIPT molecules exhibit a four-level luminescence process due to fast photo-induced tautomerization from enol* to keto* form by intramolecular proton transfer.[13] This tautomerization leads to a large Stokes shift and thereby suppresses the self-absorption.[14–16] However, existing ESIPT dyes are still unsatisfactory since they aggregate in the resonators at higher concentrations due to the high crystallinity. Actually, existing research on ESIPT dyes and their applications to laser emitters have been performed mostly in the crystalline state or in the modestly doped film state.[17,18]

Herein, we report ESIPT dyes that are miscible to spherical polymer resonators up to 50 wt%. The ESIPT dyes, **1** and a newly designed and synthesized dye **2**, feature an alkynyl chain that serves the role of enhancing the solubility, PLQY, and critical doping concentration into poly(methyl methacrylate) (PMMA) up to 50 wt% (**Figs. 1a,b**). The excessive doping (50 wt%) does not severely reduce the light confinement efficiency of the spherical WGM resonators (**Fig. 1c**). The high content of the dye provides the spheres with a higher optical gain without enhancing the optical loss due to the scattering and self-absorption, resulting in an excellent laser threshold power as low as 29 μJ cm^{-2}. The transient absorption spectroscopy and variable stripe length measurements disclose the mechanism of the optimized laser threshold, supporting the above-described molecular strategy.

The dye 2-(benzo[*d*]thiazol-2-yl)-5-(hex-1-yn-1-yl)phenol (**1**, **Fig. 1a**) was synthesized according to our previous report.[19] **1** was designed to be miscible to liquid crystalline molecules and, in the previous study, **1** can be doped into 4-pentyl-4'-cyano

[a] Department of Materials Science, Institute of Pure and Applied Sciences, University of Tsukuba, 1-1-1 Tennodai, Tsukuba, Ibaraki 305-8573, Japan.
[b] Faculty of Molecular Chemistry and Engineering, Kyoto Institute of Technology, Matsugasaki, Sakyo-ku, Kyoto 606-8585, Japan.
[c] Faculty of Electrical Engineering and Electronics, Kyoto Institute of Technology, Matsugasaki, Sakyo-ku, Kyoto, 606-8585 Japan.
[d] Department of Applied Chemistry, College of Life Sciences, Ritsumeikan University, 1-1-1 Nojihigashi, Kusatsu, Shiga 525-8577, Japan.
Electronic supplementary information (ESI) available. See DOI: 10.1039/x0xx00000x

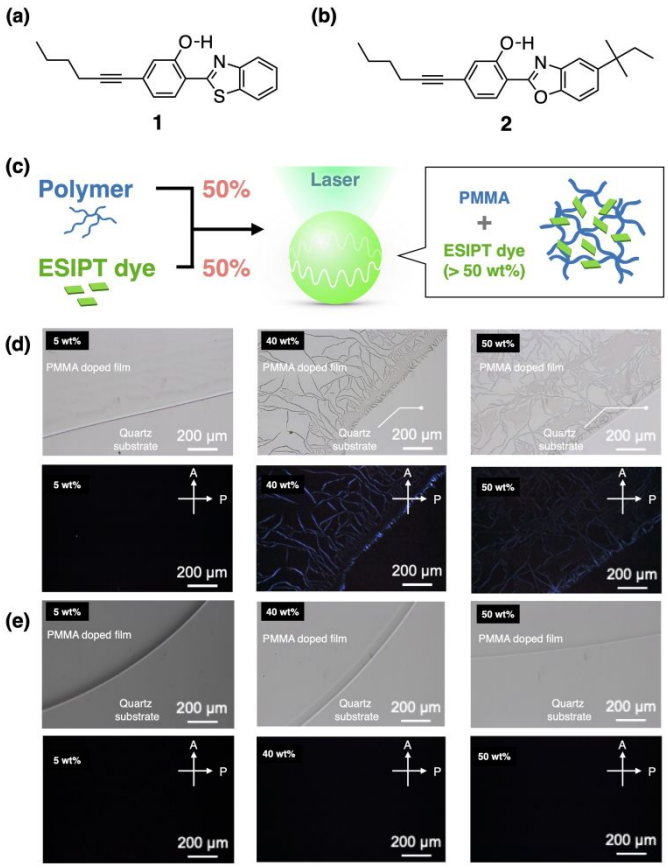

Fig. 1 (a, b) Molecular structures of **1** (a) and **2** (b). (c) A schematic representation of a spherical WGM resonator made from a polymer highly doped with ESIPT dyes. (d, e) Optical and polarized optical microscopy images at the edge of PMMA films doped with **1** (d) and **2** (e).

biphenyl (5CB) up to 15 wt%.[19] While the dye content in the host liquid crystal was high, **1** showed a relatively high PLQY up to 0.32. In the present study, we mixed the dye to PMMA for fabricating spherical optical resonators. In addition, we newly designed and synthesized 5-(hex-1-yn-1-yl)-2-(5-(*tert*-pentyl)benzo[*d*]oxazol-2-yl)phenol (**2**) featuring *tert*-pentyl group for hindering the mutual molecular aggregation (**2**, **Fig. 1b**). Starting from 2-amino-4-(*tert*-pentyl)phenol, **2** was synthesized through 2 step reactions similarly with **1** (see ESI).

We found that **1** and **2** was highly miscible to PMMA films. Typically, an aliquote of a $CHCl_3$ solution containing PMMA (100 mg mL^{-1}) and **1** or **2** was spin coated on a quartz substrate and air-dried. The weight ratio (*r*) of the dyes relative to PMMA was varied in a range from 5 to 50 wt%. The PMMA films doped with **1** were homogeneous without any visible crystalline grains in the polarized optical microscopic (POM) images with *r* below 30 wt% (**Figs. 1d, S5**). Above that value, bright domains appeared in the POM images, indicating the formation of small crystals of aggregated **1** inside the films. **2** were more miscible with PMMA, showing no visible crystalline grains in the films even at *r* of 50 wt% (**Figs. 1e, S5**). The PLQY of the PMMA films doped with **1** was nearly constant (0.35) regardless of the *r* values and the emergence of the micro-crystalline grains (**Fig. S6, Table S1**). Likewise, the average PLQY of the **2**-doped films marked 0.45 without strong dependence on *r*, validating our molecular design strategy for enhancing the miscibility as well as PLQY in the solid state. Together with the unchanged absorption and emission spectral profiles as well as PLQY upon increasing *r* (**Fig. S6, Supporting Table 1**), we conclude that the aggregation-induced emission or quenching were negligible with **1** and **2**.

Microspheres of PMMA doped with **1** (**MS^1**) and **2** (**MS^2**) were synthesized by the miniemulsion method.[3] Typically, 100 μL $CHCl_3$ solution of the dye and PMMA (5 mg mL^{-1}) was added to a 2 mL aqueous solution of sodium dodecyl sulfate (SDS, 12.5 mg mL^{-1}), and the mixture was vigorously stirred with a homogenizer at 25000 rpm for 90 s. The resulting suspension stood at 25°C for 2 days without capping for allowing $CHCl_3$ to be evaporated eventually. The precipitate was washed with H_2O through centrifugation. Fluorescent microscope (FM) and scanning electron microscope (SEM) images revealed the spherical morphology of the resulting precipitates with an average diameter of 1.14 μm (**Figs. 2a-d and S7, S8, S9**). Spherical particles predominated among the visualized precipitates when *r* was below 50 wt%. For **MS^1**, the sphericity and surface smoothness of the particles were mostly identical with each other regardless of the concentration. Besides, precipitates of **1** contained some fibrils at *r* = 50 wt% (**Fig. S10**), which is consistent with the emergence of crystalline domains in the films at higher doping concentrations (>30 wt%) as shown in **Fig. 1d**. Precipitates of **2** were spherical without any fibrils at every concentration up to 50 wt% (**Fig. S9**), while **MS^2** at *r* of 50 wt% featured a less smooth surface, indicating that 50 wt% is the upper limit of dye content in the spheres.

The microscopic photoluminescence (μ-PL) spectra from a single sphere were measured by a homemade microscope system equipped with a ns-laser (λ = 355 nm) for the optical excitation of the particle. Spheres without any visible agglomeration with the others were selected for the measurements for better reproducibility. The μ-PL spectrum of **MS^1** with *r* = 5 wt% (**MS$^1_{5\%}$**) showed periodic sharp peaks overlapping on the broad emission band (**Fig. 2e**). The sharp peaks are assignable to the series of transverse electric (TE) and magnetic (TM) modes of WGM optical resonance, which is corroborated by the linearity of the free spectrum range (FSR) plotted against the inverse of the diameter of the sphere observed (**Fig. S11**).[20,21] Spectra with an essentially identical features were also observed with **MS$^2_{5\%}$** (**Fig. S12**).

We found that the WGM peaks appear even at the shorter-wavelength shoulder of the spontaneous emission band. The WGM peaks were visible in a wavelength range from 470 to 510 nm for **MS$^1_{5\%}$** and from 440 to 480 nm for **MS$^2_{5\%}$**. These peaks are usually undetectable with the typical organic WGM resonators, since the shorter wavelength region of the emission band overlaps with the edge of the absorption band, resulting in the severely attenuated WGM peaks due to the self-absorption.[22] In contrast, the self-absorption of **1** and **2** is almost negligible due to the large Stokes shift, thereby making the WGM peaks visible even in the shorter wavelength region.

The light confinement efficiencies of **MS^1** and **MS^2** were analysed based on the μ-PL spectra. *Q*-factor is a representative figure-of-merit of an optical resonator, defined as the peak

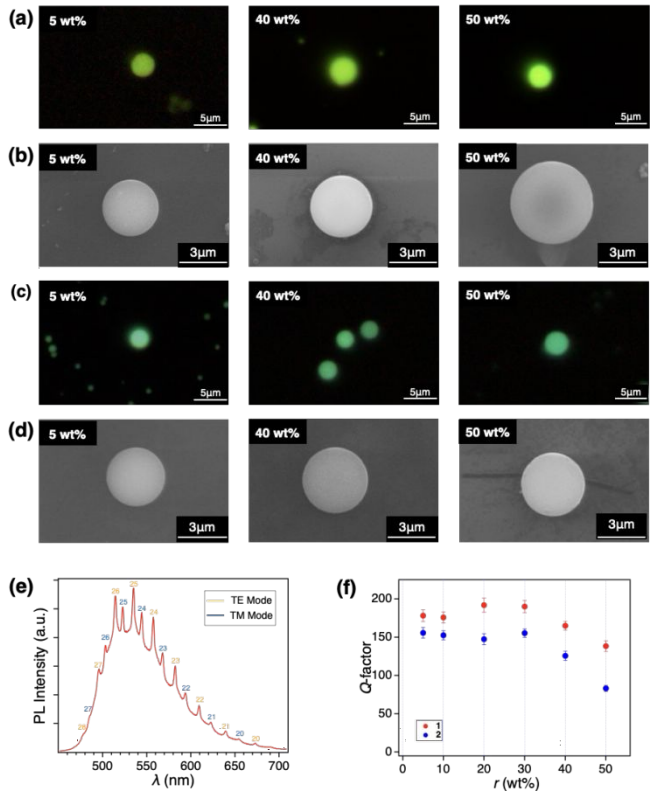

Fig. 2 (a–d) Fluorescent (a, c, λ_{ex} = 350 nm) and scanning electron microscopy (b, d) images of **MS¹** and **MS²**. (e) μ-PL spectrum of **MS¹$_{5\%}$**. The TE and TM mode numbers of the WGM resonance are indicated in orange and blue, respectively. (f) Plots of *Q*-factors versus *r* in **MS¹** (red circles) and **MS²** (blue circles) with error bars (standard deviations, *n* = 10)

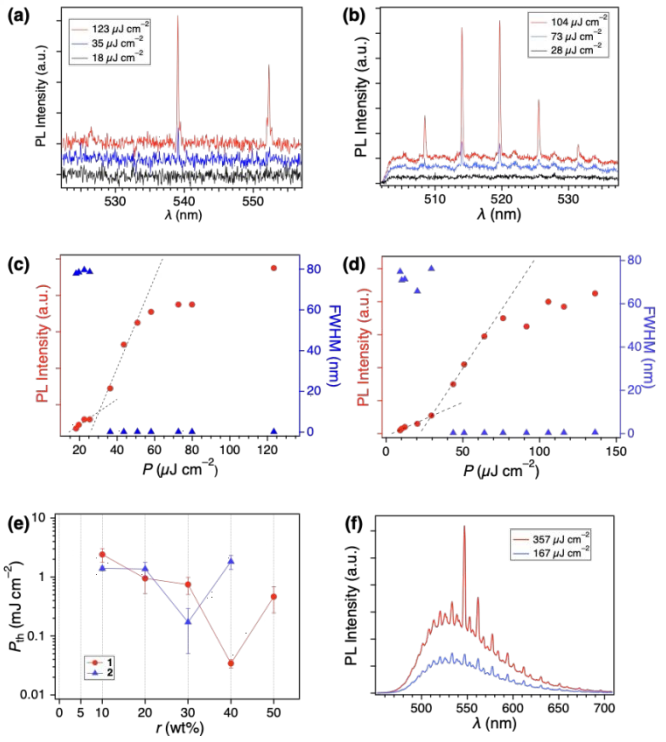

Fig. 3 (a, b) μ-PL spectra of **MS¹$_{40\%}$** (a) and **MS²$_{30\%}$** (b) upon pumping with fs-laser. (c, d) Plots of PL intensities (red circles) of a peak of **MS¹$_{40\%}$** at 539 nm (c) and **MS²$_{30\%}$** at 514 nm (d) and their full-width-at-half-maxima (FWHM, blue triangles) versus power density (*P*) of the excitation light. The dashed lines indicate the regression lines of the PL intensities below and above the lasing threshold, providing the lasing threshold power density (P_{th}) as their crossing point. (e) Semilogarithmic plots of P_{th} of **MS¹** (red circles) and **MS²** (blue triangles) versus *r*. The error bars represent standard deviation (*n* = 5). (f) μ-PL spectra of **MS¹$_{40\%}$** upon pumping with a ns-laser.

wavelength divided by its full width at the half maximum (FWHM).[23] **Fig. 2f** shows the plots of the average *Q*-factors of **MS¹** and **MS²**, showing a plateau up to *r* = 30 wt% and a subsequent downward trend for both specimens. The constant *Q*-factor up to *r* = 30 wt% ensures the efficient light confinement in **MS¹** and **MS²**, while the efficiency gradually deteriorated upon further increase of the dye contents, which is plausibly due to the partial aggregation of the dye and the roughed surface of the spheres.[22] Nonetheless, the resonance peaks were still visible and sharp even at *r* = 50 wt% by virtue of the high miscibility of **1** and **2**.

We found that the spheres showed laser oscillation upon strong optical pumping. The pumping was conducted with a fs-laser (Δ: 80 fs, repetition rate: 1 kHz) that was focused onto the spheres through a lens (*f*: 120 mm, spot size: 50 μm). The emission was collected with an optical fibre (*d* = 200 μm, N.A. 0.22) through an objective lens (x20, N.A. 0.40). The spheres were dropcast on a quartz substrate and, after air-drying, subjected to the irradiation of the fs-laser pulses. At stronger pumping, the PL spectra of **MS¹$_{40\%}$** showed sharp peaks (**Figs. 3a, c**) with an average lasing threshold power density (P_{th}) of 30 μJ cm^{-2}. Concomitantly, the peaks were sharpened drastically down to 0.19 nm. The higher laser intensities of **MS²** when compared to **MS¹** at higher *P* is likely due to the higher PLQY of **2** (**Supporting Table 1**), leading to the higher gain saturation.

The smaller *Q*-factor at higher *r* usually indicates inferior laser performance. However, this may not be true for **MS¹** and **MS²** since the gain increases at higher *r* and may compete with the decrease in *Q*-factor. Actually, we observed the lasing spectra of **MS¹** and **MS²** with *r* of 5–50 wt% (**Figs. 3a–d**). The obtained average P_{th} values are plotted in **Fig. 3e**. Notably, the average P_{th} of **MS¹$_{40\%}$** was 70 times smaller than that of **MS¹$_{10\%}$**. The smallest average P_{th} (34 μJ cm^{-2}) was achieved at *r* = 40 wt%. A similar trend was also observed with **MS²**. We surmise that the higher dye concentration in the resonator increases the optical gain per unit length without increasing the optical loss due to the self-absorption. Observation with variable stripe length methods supported this hypothesis (**Fig. S13**, see ESI for the details of the experiments).[24] We also noticed that the trend was not monotonic, showing an increase in P_{th} at higher *r* (**Fig. 3e**). As discussed in **Fig. 2f**, too much doping induced the decrease in *Q*-factor. We consider that the decrease in *Q*-factor was more fatal than the increase in the gain at higher *r* regain (*r* > 40 and 30 wt% for **MS¹** and **MS²**, respectively), leading to the non-monotonic trend of P_{th}.

We also examined the overlap of the excited-state absorption with the emission band, which usually gives negative effect to P_{th}. The excited-state dynamics of **1** were investigated with transient absorption spectra.[25,26] PMMA films doped with **1** (*r* = 10–30 wt%) and a CH_2Cl_2 solution of **1** (0.1 mg mL^{-1}) were excited with 347 nm-laser pulses, and the transient absorption spectra were measured. The difference spectra showed an excited-state absorption at 400–460 nm, which are formed

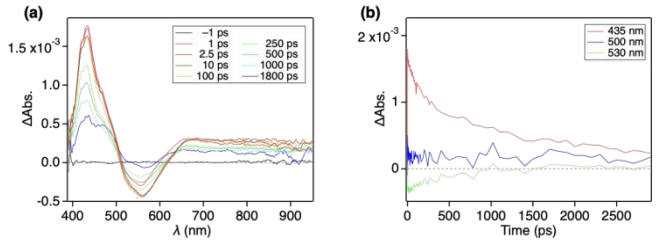

Fig. 4 (a) Transient absorption spectra of a PMMA film doped with **1** (r = 30 wt%) photoexcited at 347 nm (100 nJ pulse^{-1}). (b) Time-dependent changes of differential absorbance (ΔAbs.) at wavelengths of 435, 500 and 530 nm.

within the instrumental response function (~100 fs) and decayed with a time constants of 1.2×10^2 (33.4%) and 1.1×10^3 (66.6%) ps (**Figs. 4b, S14**). The profiles were analogous to the conventional ESIPT dyes, and, accordingly, the band at 400–460 nm was attributed to the keto* form of **1** (**Figs. 4a, S14**).[25,26] The band was barely overlapped with the stimulated emission band centred at 530 nm, contributing to the suppressed effect due to the excited-state re-absorption.

As is summarized in a previous review paper,[27] fs-lasers as an excitation source, are not convenient for most industrial and daily usages due to the large footprint and the machine complexity. Alternatively, ns-lasers are concise and commercially more available. Along this context, we conducted strong optical pumping experiments with a ns-laser instead of the fs-laser. As shown in **Figs. 3f** and **S14**, $\mathbf{MS^1_{40\%}}$ and $\mathbf{MS^2_{30\%}}$ showed lasing peaks in analogy with those observed upon pumping with the fs-laser, demonstrating its potential for future applications. However, the lifetime of the lasing was considerably shorter, and P_{th} was not observable due to the fast degradation of the dye, which will be optimized in the future study by means of molecular design.

In summary, we demonstrated the high miscibility of **1** and **2** to a polymer matrix and their applicability to low-threshold spherical laser oscillators. Excessive doping of **1** and **2** did not induce visible aggregation of the dyes, enhancing the optical gain of the microspheres. In addition, the ESIPT property of the dyes suppressed the self-absorption and contributed to the significantly low lasing threshold. This study provides a new molecular design for the development of low-threshold organic lasers with spherical morphology and high dye content.

Conflicts of interest

There are no conflicts to declare.

Data availability

The data supporting this article have been included as part of the ESI.

Acknowledgements

This work was financially supported by CREST (JPMJCR20T4), ACT-X (JPMJAX201J), and FOREST Programs (JPMJFR232J) from JST, and KAKENHI (JP22K14656, JP23KK0099, JP24H00470, JP24H01693, JP23H01935) from JSPS.

Notes and references

1 W. Zhang, J. Yao and Y. S. Zhao, *Acc. Chem. Res.*, 2016, **49**, 1691.
2 G. C. Righini and S. Soria, *Sensors*, 2016, **16**, 905.
3 Y. Yamamoto, D. Okada, S. Kushida, Z. S. Ngara and O. Oki, *J. Vis. Exp.*, 2017, e55934.
4 Z. Xu, Q. Liao, X. Wang and H. Fu, *Adv. Opt. Mater.*, 2014, **2**, 1160.
5 Y. Wei, X. Lin, C. Wei, W. Zhang, Y. Yan and Y. S. Zhao, *ACS Nano*, 2017, **11**, 597.
6 G.-Q. Wei, X.-D. Wang and L.-S. Liao, *Laser Photon. Rev.*, 2020, **14**, 2000257.
7 T. G. Pavlopoulos, *Prog. Quantum Electron.*, 2002, **26**, 193.
8 A. François, N. Riesen, H. Ji, S. Afshar V. and T. M. Monro, *Appl. Phys. Lett.*, 2015, **106**, 031104.
9 Y. Zhang, D. Li, Y. Ou, X. Pu and Y. Sun, *IEEE Photonics J.*, 2019, **11**, 1.
10 M. J. Currie, J. K. Mapel, T. D. Heidel, S. Goffri and M. A. Baldo, *Science*, 2008, **321**, 226.
11 F. Rezaei, G. Cristoforetti, E. Tognoni, S. Legnaioli, V. Palleschi and A. Safi, *Spectrochim. Acta Part B At. Spectrosc.*, 2020, **169**, 105878.
12 A. V. Yakuhina, A. S. Kadochkin, D. V. Gorelov, V. V. Svetukhin, S. S. Generalov and V. V. Amelichev, *Photonics*, 2021, **8**, 225.
13 A. Weller, *Naturwissenschaften*, 1955, **42**, 175.
14 S. Park, J. E. Kwon, S. H. Kim, J. Seo, K. Chung, S.-Y. Park, D.-J. Jang, B. M. Medina, J. Gierschner and S. Y. Park, *J. Am. Chem. Soc.*, 2009, **131**, 14043.
15 D. A. Yushchenko, V. V. Shvadchak, A. S. Klymchenko, G. Duportail, V. G. Pivovarenko and Y. Mély, *J. Phys. Chem. A*, 2007, **111**, 10435.
16 C.-C. Yan, Y.-P. Liu, W.-Y. Yang, J.-J. Wu, X.-D. Wang and L.-S. Liao, *Angew. Chem. Int. Ed.*, 2022, **61**, e202210422.
17 G.-Q. Wei, Y. Yu, M.-P. Zhuo, X.-D. Wang and L.-S. Liao, *J. Mater. Chem. C*, 2020, **8**, 11916.
18 J. Massue, T. Pariat, P.-M. Vérité, D. Jacquemin, M. Durko, T. Chtouki, L. Sznitko, J. Mysliwiec and G. Ulrich, *Nanomaterials* 2019, **9**, 1093.
19 W. Zhang, S. Suzuki, S. Cho, G. Watanabe, H. Yoshida, T. Sakurai, M. Aotani, Y. Tsutsui, M. Ozaki and S. Seki, *Langmuir*, 2019, **35**, 14031.
20 A. Qiagedeer, H. Yamagishi, S. Hayashi and Y. Yamamoto, *ACS Omega*, 2021, **6**, 21066.
21 K. Tabata, D. Braam, S. Kushida, L. Tong, J. Kuwabara, T. Kanbara, A. Beckel, A. Lorke and Y. Yamamoto, *Sci. Rep.*, 2014, **4**, 5902.
22 O. Oki, S. Kushida, A. Mikosch, K. Hatanaka, Y. Takeda, S. Minakata, J. Kuwabara, T. Kanbara, T. D. Dao, S. Ishii, T. Nagao, A. J. C. Kuehne, F. Deschler, R. H. Friend and Y. Yamamoto, *Mater. Chem. Front.*, 2018, **2**, 270.
23 S. Schiller, *Appl. Opt.*, 1993, **32**, 2181.
24 L. D. Negro, P. Bettotti, M. Cazzanelli, D. Pacifici and L. Pavesi, *Opt. Commun.*, 2004, **229**, 337.
25 Y. Yang, Q. Zhang, Y. Liu, Z. Jiang, C. Qin, K. Jiang and Y. Liu, *J. Lumin.*, 2022, **248**, 118922.
26 M. Iravani and R. Omidyan, *J. Phys. Chem. A*, 2018, **122**, 3182.
27 S. Chénais and S. Forget, *Polym. Int.*, 2012, **61**, 390.

Data availability statement

The data supporting this article have been included as part of the electronic supplementary information.